Electrochimica Acta 477 (2024) 143780

Contents lists available at ScienceDirect

Electrochimica Acta

journal homepage: www.journals.elsevier.com/electrochimica-acta

An electroplated Ag/AgCl quasi-reference electrode based on CMOS top-metal for electrochemical sensing

Lewis Keeble [a,*], Arthur Jaccottet [a,b], Daryl Ma [a], Jesus Rodriguez-Manzano [c], Pantelis Georgiou [a]

[a] Centre for Bio-inspired Technology, Department of Electrical and Electronic Engineering, Imperial College London, London, SW7 2AZ, UK
[b] Microengineering Section, École Polytechnique Fédérale de Lausanne, Lausanne, 1015, Switzerland
[c] Department of Infectious Disease, Faculty of Medicine, Imperial College London, London, SW7 2AZ, UK

ARTICLE INFO

Keywords:
CMOS
Reference electrode
Electroplating
Electrochemical
Electroless

ABSTRACT

The integration and mass-production of reference electrodes for CMOS-based electrochemical sensing systems pose a challenge for the accessibility and commercial-viability of such devices. In this paper, a method of electroplating an Ag/AgCl quasi-reference electrode using CMOS top-metal as a base is presented for the first time. The aluminium bond-pad of a CMOS microchip was zincated, an electroless nickel immersion gold layer applied, and a thick silver layer electroplated and chemically chlorinated. The resulting reference electrode was able to provide a stable potential with a drift rate of 0.3 mV/h for up to 18 h. This validates the approach of a fully electroplated bond-pad reference electrode, which offers simplified post-processing and greater scalability of production. Further work towards an entirely electroless process is envisaged.

1. Introduction

Electrochemical sensing methods have a wide range of applications, including medical biosensing, environmental monitoring, and food analysis [1]. Electrochemical sensing is ideally-suited to implementation on complementary metal–oxide–semiconductor (CMOS), which offers benefits to device cost, performance, and portability [2,3]. Many electrochemical detection systems require a reference potential to either bias field-effect transistors (FETs and ISFETs) or reliably measure working electrode (WE) potential in three-electrode systems. The reference electrode (RE) that produces this potential must be able to keep it stable over time; Any fluctuations or drift in reference potential will obscure the electrochemical signal. However, the integration of conventional REs poses a challenge for CMOS-based systems due to the small sample volumes encountered when microfluidic sample handling approaches are used.

The most popular RE for electrochemical sensing applications, is silver/silver chloride (Ag/AgCl), due to its stability, robustness, and relatively simple and inexpensive construction [4]. The chemical reaction that defines the behaviour of the Ag/AgCl RE is,

$$AgCl(s) + e^- \rightleftharpoons Ag(s) + Cl^-(aq) \quad (1)$$

Ag/AgCl Quasi-REs (QRE), where local chlorine (Cl) ion concentration is not controlled, have simpler constructions at the expense of reference potential stability and longevity [5–7]. Fabrication approaches for miniaturised QREs fall into three main categories:

- **Thin-Film:** The development of photo-patterned structures on a substrate combined with deposition of metal through sputtering or evaporation [8–10].
- **Inkjet printing:** Deposition of metallic inks, often nanoparticle suspensions, through specialised printing equipment [11–13].
- **Screen printing:** Deposition of metallic pastes that are pushed through a patterned mesh [14,15].

Screen printing, whilst cheap and straightforward, lacks resolution in its metal deposition. Inkjet printing allows fast and scalable electrode production, yet also suffers from poor deposition resolution and requires expensive equipment and materials. Thin-film approaches to QRE fabrication offer the best resolution in metal deposition, but require more processing, expensive equipment, and a controlled environment.

Thin-film fabrication is the most common approach to producing on-CMOS REs [3]. The native CMOS process includes passivation (pad) openings, where windows are etched in the insulation that covers the microchip, exposing the top-metal layer underneath. By fabricating the RE on these bond-pads, the electrical connection to the RE can be made as the part of the integrated circuitry that is buried underneath the passivation. This makes subsequent encapsulation of the sensing system significantly more straightforward. Ag/AgCl QREs have been fabricated on CMOS bond-pads through sputtering or evaporation of silver (Ag), which is then chlorinated to form AgCl [6,7]. As an alternative, many

* Corresponding author.
E-mail address: l.keeble18@imperial.ac.uk (L. Keeble).

https://doi.org/10.1016/j.electacta.2024.143780
Received 3 November 2023; Accepted 3 January 2024
Available online 6 January 2024

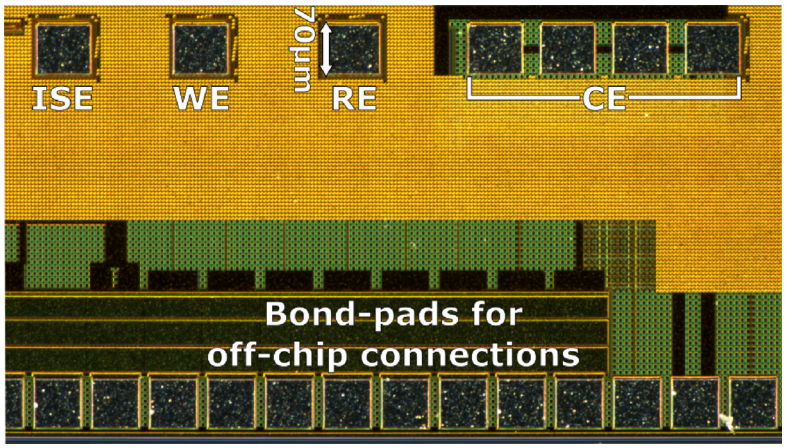

Fig. 1. Micrograph of the 0.18 μm TSMC microchip used as a test platform in this study. The pads for the ISE, WE, RE, and CE are highlighted.

studies use pseudo-reference electrodes (PREs), where no half-cell exists between electrode and electrolyte, consisting of gold [16,17] or platinum [18]. Using PREs simplifies the fabrication process, but provides sub-optimal sensing compared to QREs and can only be applied in well-controlled environments.

Sputtering and evaporation are ill-suited to deposit thick layers of Ag in the order of microns. The thickness of the Ag layer will determine the amount of AgCl available after chlorination of the surface. This, in turn, is the limiting factor in a QRE's lifetime, as it will not be able to hold a stable potential after all AgCl has dissolved. Some studies use a dissolution-limiting coating over a QRE to extend its lifetime [19–21], but this is not necessary if the AgCl layer is sufficiently thick.

Electroplating is ideal for producing thick layers of metals through electrochemical reactions and requires little in the way of set-up. This is particularly the case for electroless plating, which occurs without an applied current and can be conducted at scale. However, electroplating on its own cannot produce a QRE — A metallic base is required upon which to electroplate. This base is most commonly provided via sputtering or evaporation of metal. Alternatively, the standard aluminium (Al) bond-pads of commercial CMOS processes could be used as a base for electroplating an on-chip Ag/AgCl QRE, instead of sputtering additional layers. Such a fabrication process would consist of simple steps, require little in the way of equipment, and could be manufactured at scale. This would contribute to the accessibility and commercial viability of CMOS-based electrochemical sensing devices.

This paper will demonstrate the fabrication of a fully electroplated Ag/AgCl QRE using standard CMOS bond-pads as a base for the first time. This paper will then show that such an electrode is capable of producing a stable reference potential over long measurement times. The ultimate vision is to have an entirely electroless fabrication process, whereby QRE production can occur on a multi-wafer level, far outstripping the scale of other methods.

2. Material and methods

2.1. CMOS test platform

A CMOS microchip fabricated in 0.18 μm TSMC was used as a test platform for the Ag/AgCl bond-pad QRE fabrication process [22]. The chip contains seven Al bond-pads within the interior of the chip as part of a four-electrode voltammetry-amperometry sensing system, consisting of: an ion-sensitive electrode (ISE), a RE, a WE, and a counter electrode (CE, four connected pads), as seen in Fig. 1. These are connected as part of the IC to bond-pads on the edge of the chip to allow external connection.

Prior to electroplating, the dies were glued to a PCB with silver epoxy (*Epotek*), wirebonded using a wedge wirebonder (*F&S 53*), and the wires covered in black epoxy (*Epotek*). The PCB was also coated in black epoxy to protect the tracks and vias from the plating baths.

2.2. Fabrication process

2.2.1. Zincation

Electroplating directly on to Al is prohibited by an aluminium oxide (Al_2O_3) layer that causes poor adhesion. Al oxidises so readily, that even if this oxide layer was etched away, it would reform before any subsequent plating could occur [23]. Therefore, it is common practice to immediately replace the surface Al with a metal that is more resistant to oxidisation, with zincate being the most widely used Al treatment. Techni Zincate (*Technic UK*) was used in this study.

Prior to zincation, the chip was cleaned with acetone (*Sigma*) and isopropanol (*ThermoFisher*) in an ultrasonic bath for 10 min and the surface was activated by immersing the chip in 1 M hydrochloric acid (HCl) for 10 min. The Al_2O_3 layer was etched with a 5 s immersion in 5% sodium hydroxide (NaOH, *Sigma*). Short etching times were used to avoid complete dissolution of the Al pad [24]. The bond-pads of 0.18 μm TSMC are made of Al that contains a low (~ 5%) percentage of copper (Cu). This Cu can form precipitates during etching that will affect the adhesion of subsequently deposited metal layers. This Cu 'smut' was removed with a 5 s immersion in 50% nitric acid (HNO_3, *Sigma*) and the zincate solution was then applied immediately with a 150 s immersion time.

A double zincation process was used, whereby the first zinc (Zn) layer was stripped away with a 3 s immersion in 50% HNO_3, after which another Zn layer was applied with a 50 s immersion in the plating solution. The aim of a double zincation is to improve the smoothness of the Zn layer [23].

2.2.2. Electroless nickel immersion gold

Ag is most commonly electroplated on to nickel (Ni) or Cu. However, in Polk et al. 2006 a gold (Au) intermediary layer was used as a barrier to prevent the diffusion of metal oxides in to the Ag layer [25] and the changes in reference potential they would cause. Electroless nickel immersion gold (ENIG) is a well-established, industry-standard process used to create Au bump-pads or electrodes on CMOS dies [24,26,27] and form solder pads on PCBs.

The electroless Ni is an autocatalytic plating process, where the Ni layer grows continually. Techni EN AT 5600 (*Technic UK*) was used in this study and is a three-part, cyanide-free electroless Ni plating solution. The plating solution was heated to 85 °C with stirring provided by a magnetic stirrer at 350 rpm (CRS 22H hotplate). The plating was conducted for up to 18 min, with a predicted plating rate of 10–15 μm/h.

The immersion Au process is a displacement reaction through which Au atoms replace all surface Ni atoms, at which point the reaction terminates, providing only a thin layer of Au. Supermex 250 (*Metalor*) was used in this study and is a cyanide-free, ready-to-use immersion Au plating solution. The plating solution was heated to 65 °C with

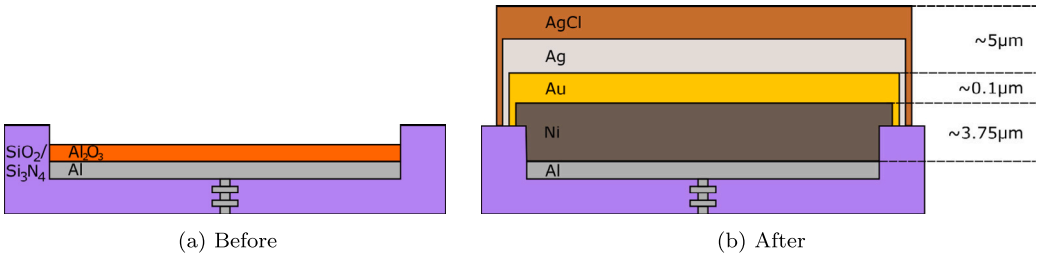

Fig. 2. A schematic showing the composition of the pad (**a**) before and (**b**) after post-processing, with the approximate thicknesses of the electroplated layers provided.

stirring provided by a magnetic stirrer at 200 rpm (*CRS 22H*). Plating was conducted for up to 25 min, providing a maximum thickness of 0.1 μm.

2.2.3. Electroplated silver

For Ag deposition on the immersion Au surface, there is currently no commercially available autocatalytic process. Immersion finishes are inherently limited in the thicknesses they can provide and they may not deposit sufficient Ag to create a QRE with a realistically usable lifetime. Consequently, current-driven Ag plating was conducted in this study.

As opposed to having the plating current applied constantly, more uniform Ag coverage can be achieved by pulsing the current [28]. When the current is active, Ag ions will be removed from the solution, leading to its depletion. By turning off the current, Ag ions are given time to diffuse from the bulk solution and evenly distribute across the metal surface. This leads to smoother plating with smaller Ag grain sizes. A pulsed current of 13 mA/cm with 2 s on and 20 s off is used, with 10 min total of applied current.

The Ag plating solution used in this study was 0.3 M silver nitrate ($AgNO_3$, *ThermoFisher*) dissolved in 1 M ammonium hydroxide (NH_4OH, *Sigma*). An Ag wire was used as a RE, a platinised titanium mesh was used as a counter electrode, and the three-electrode system was run using a VersaStat 3 electrochemical workstation. Prior to electroplating the surface was activated by immersing the chip in 1 M hydrochloric acid (HCl) for 10 min [25].

2.2.4. Silver chlorination

To complete the QRE the Ag layer must be chlorinated to convert the surface to AgCl. This AgCl layer creates the half-cell between QRE and test solution that ensures stability of the reference potential. There are two main approaches to the chlorination of Ag: Chemical oxidation and electro-chemical anodisation, whereby a current is applied to the Ag in an aqueous solution of a chloride salt. Both methods have been found to produce equally stable QREs [25]. For the purpose of wafer-level fabrication, chemical oxidation is preferential because it does not require an electrical connection. Iron (III) chloride ($FeCl_3$, *Sigma*) was chosen as the chemical oxidiser and an immersion time of 60 s was used, with chlorination occurring immediately after plating.

The final composition of the electrode produced via this process is illustrated in Fig. 2. More information regarding the optimisation of this fabrication process can be found in the supplementary material.

2.3. Characterisation

2.3.1. Microscopy

Brightfield microscopy was conducted with a Nikon Eclipse LV100. Scanning electron microscopy (SEM) was carried out using a Lyra Tescan G3, with concurrent energy-dispersive X-ray (EDX) analysis. EDX is a technique for identifying elemental presence on a surface via the spectra of X-rays emitted during electron beam bombardment.

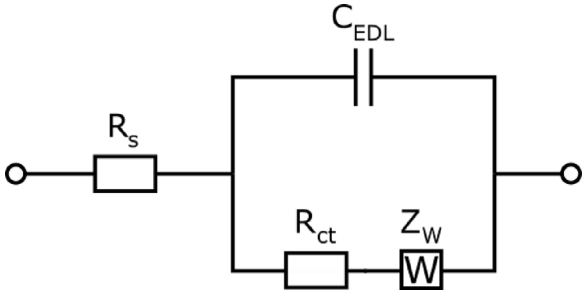

Fig. 3. An equivalent circuit diagram of the Randles circuit. R_s is the electrolyte resistance, C_{EDL} is the EDL capacitance, R_{ct} is the charge transfer resistance, and Z_W is an impedance element that represents a faradaic reaction.

2.3.2. Profilometry

A Dektak 6M Veeco stylus profilometer was used to provide surface profiles of bare, ENIG-plated, and Ag-plated bond-pads. This allowed estimation of layer thicknesses.

2.3.3. Electrochemical characterisation

The open circuit potential (OCP) of an electrochemical system is the potential when no external load is applied and no current flows. A two-electrode set-up (*VersaStat 3*) was used, with the potential of the working electrode measured relative to the RE. The measured potential will be determined by the electrolytic activity at the working electrode. OCP is a useful measure of the drift in the QRE and its lifetime, as the AgCl layer corrodes during measurement. OCP was measured in 100 mM potassium chloride (KCl, *Scientific Laboratory Supplies*), with the electroplated Ag/AgCl pad as the WE and a commercial, glass Ag/AgCl RE (Sigma).

Cyclic voltammetry (CV) is a useful tool for characterising electron transfer processes by subjecting an electrochemical system to a sweep in voltage and measuring the current induced by redox reactions at the electrode surface. The peak value of current, i_p, is related to the scanning rate, υ, at which the voltage is swept, by the Randles–Cevcik equation,

$$i_p = 0.446nFAc_0\sqrt{\frac{nF\upsilon D_o}{RT}} \tag{2}$$

where F is the Faraday constant, n is the number of electrons involved in reduction, D_o is the diffusivity of the oxidised molecule, c_0 is the bulk analyte concentration, A is the area of the electrode, and T is the temperature of the system. By varying the scan rate of the CV curves, a linear relationship between i_p and $\sqrt{\upsilon}$ will indicate that the reaction is diffusion-limited and electron transfer at the electrode surface is fast, as is desired.

Another important feature in interpreting CV curves is the peak-to-peak separation of the anodic (i_p^a) and cathodic (i_p^c) peaks, which is

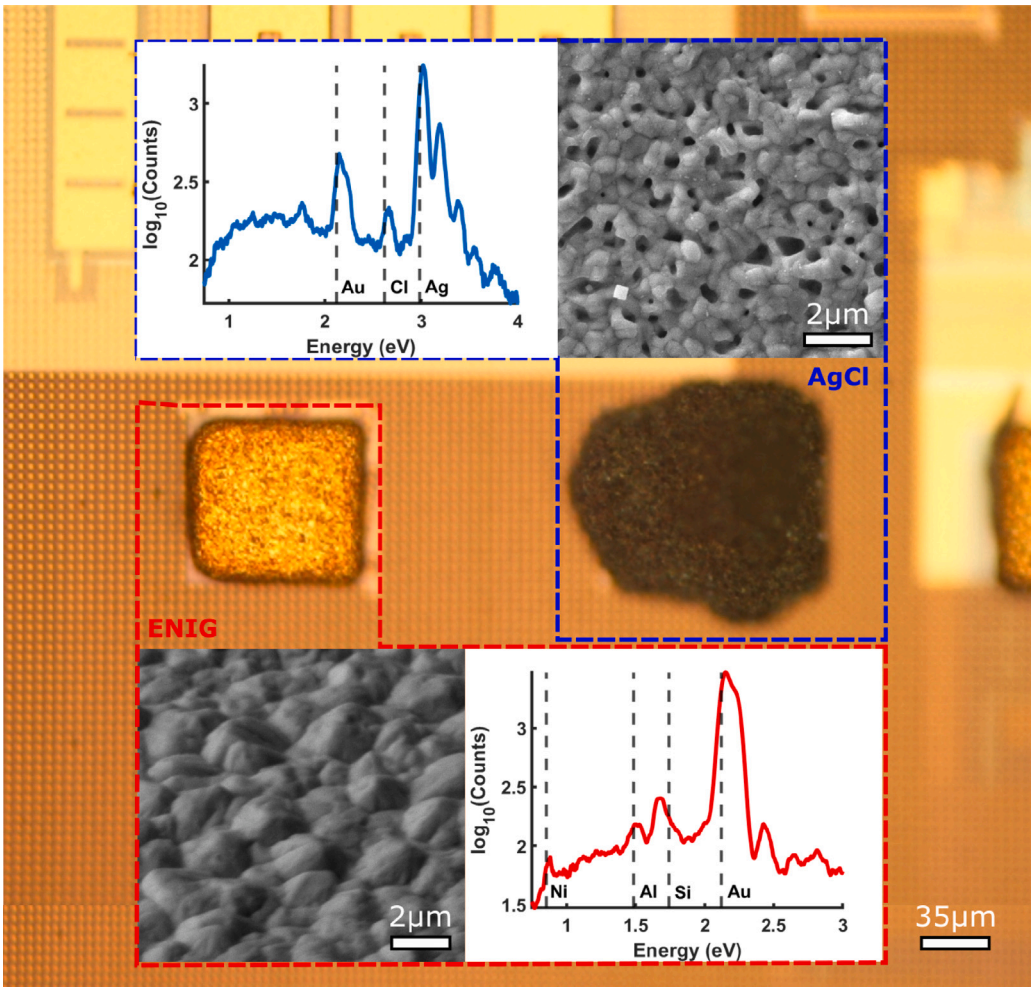

Fig. 4. A microscope image of an ENIG-plated and an AgCl-plated pad. SEM close-up images of the surface topology were obtained with a beam energy of 10 kV. White scale bars are provided for the microscope and SEM images separately. EDX spectra of the surfaces are provided, annotated with the elements corresponding to certain peaks.

57 mV in the ideal case [29]. Measurement of the peak ratio is complicated by the inherent hysteresis present in CV cycles. The switching voltage influences the value of the anodic peak and, as such, its raw value cannot be used. An empirical model for peak ratio,

$$R = \frac{i_p^c}{i_p^a} + 0.48\frac{i_\lambda}{i_p^a} + 0.086 \tag{3}$$

was determined by Nicholson et al. [30], where i_λ is the current at the switching voltage and $R = 1$ in the ideal case.

CV was conducted in a solution of 0.1 M KCl, 0.1 mM potassium ferricyanide, and 1 mM potassium ferrocyanide (K_3FeCN_6 and K_4FeCN_6 respectively, both *Sigma*). A three-electrode set-up (*VersaStat 3*) was used, with a commercial, glass Ag/AgCl RE and a platinised titanium mesh CE. An ENIG-coated pad was used as the WE, which was then plated with AgCl and testing repeated. In doing so, the electrochemical performance of the underlying ENIG layer was separated from that of the full Ag/AgCl electrode. The electrochemical set-up was placed in a grounded Faraday cage to reduce noise from the surrounding environment.

Impedance analysis is another method to characterise the charge-transfer properties of an electrode. The impedimetric interaction between an electrode and electrolyte can be modelled with the Randles equivalent circuit, displayed in Fig. 3. Fitting of this circuit to experimental data allows the determination of the charge transfer resistance, R_{ct}. A high R_{ct} will limit the speed with which a RE can respond to changes in environmental conditions.

Impedance spectra were obtained using a 3-electrode set-up (*CHI760E Electrochemical Workstation*), with an ENIG or Ag/AgCl pad as the WE, a commercial glass RE, and a platinised mesh CE. Spectra were obtained within 100 mM KCl from 10 Hz to 100 kHz with a 5 mV applied voltage. Fitting of the Randles circuit was conducted within the workstation software.

3. Results

3.1. Fabricated prototypes

ENIG plating was successfully conducted, as exemplified by Fig. 4, with the presence of Au confirmed by EDX analysis of the surface. The surface profile data contained in Fig. 5 demonstrates that the ENIG layer has risen above the passivation layer, creating the expected 'bump' profile.

To verify the adhesion of the underlying layers, tape tests were performed, with adhesive Kapton tape applied to the bond-pad and removed. In the majority of attempts, no delamination of the ENIG coating occurred. However, where delaminations did occur, analysis of the pad using SEM found that in most instances the underlying Al pad had delaminated from the array of vias connecting it to the circuitry underneath. This suggests that the adhesion of the ENIG layer is good, but it is also possible that over-etching of the pad during the zincation step has resulted in the weakening of the Al layer.

Ag was successfully plated and chlorinated, as shown in Fig. 4, with the presence of both Ag and Cl confirmed by EDX analysis. The final

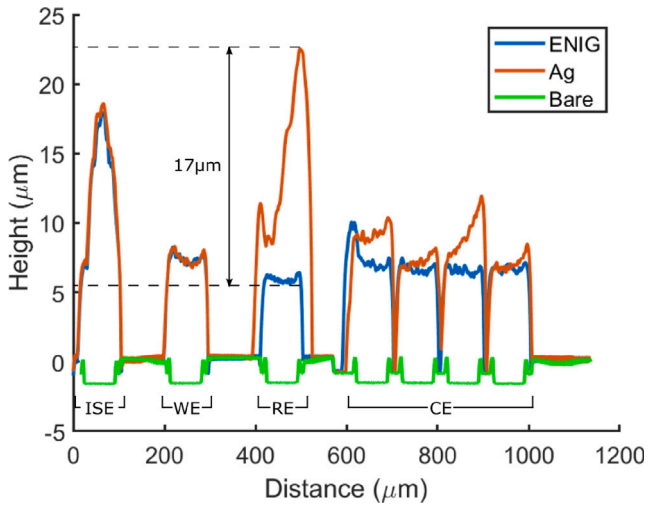

Fig. 5. Surface profiles of the DAPPER ion-sensitive (ISE), working (WE), reference (RE), and counter (CE) electrodes. Profiles are shown for the bare chip and the chip after ENIG plating of all electrodes and Ag plating of the RE pad only.

Table 1
Parameters for CV experiments on the ENIG and Ag/AgCl-coated pads, averaged over all scan rates.

Parameter	Ideal	ENIG pad	AgCl pad
Peak-to-Peak	57 mV	163.6 mV	336.3 mV
Peak Ratio	1	0.9198	2.4874

Ag/AgCl layer showed good adhesion, as it passed all tape tests. The surface profile of an Ag-plated RE, shown in Fig. 5, indicates that the Ag layer is between 5 - 17 μm thick.

3.2. Electrochemical performance

The OCP of one of the fabricated QREs is shown in Fig. 6. The potential varied between 75 - 65 mV over 18 h of measurement, with an overall drift rate of 0.3 mV/h. A large discontinuity can be seen at around 7 h which is believed to be caused by bubble formation.

CV data for the ENIG and Ag/AgCl-coated pads is provided in Fig. 7, with the key parameters compiled in Table 1. For the Ag/AgCl-coated pad, the non-linear $i_p^c - \sqrt{v}$ relationship and the peak-to-peak separation and peak ratio being larger than ideal suggests slow electron transfer. However, the CV spectrum for the Ag/AgCl electrode will be dominated by the reaction shown in Eq. (1), with peak current densities almost three orders of magnitude larger than observed for the ferro/ferricyanide system using the ENIG-coated pad.

In comparison, the underlying ENIG layer demonstrates superior electron transfer properties. The noise on the signal is high, because the currents being measured from the microelectrode are in the order of 10 nA and thus interference from the surroundings is comparatively large.

The impedance data shown in Fig. 8 and the fitted Randles circuit parameters contained in Table 2 demonstrate the increase in electrode impedance of the final Ag/AgCl-plated pad compared to the ENIG-plated. The Nyquist plot for the Ag/AgCl pad exhibits short (finite-length) Warburg behaviour at low frequencies, indicating the porous properties of the AgCl layer. R_{ct} is higher for the Ag/AgCl pad, likely caused by the increased thickness of the metal coating or the presence of oxidised Ag. C_{EDL} is reduced for the Ag/AgCl pad, demonstrating the reduced polarisation that it exhibits. R_{ct} in the order of kΩ and C_{EDL} in the order of nF is comparable to values in the literature [25,31].

Table 2
Parameter values of the Randles circuit in Fig. 3 as fitted to the impedance spectra shown in Fig. 8 for the ENIG and Ag/AgCl-plated pads.

Electrode	R_s (kΩ)	R_{ct} (kΩ)	C_{EDL} (nF)	Z_W ($\mu\Omega\sigma^{-\frac{1}{2}}$)	χ^2
ENIG	1.216	1.867	1.577	43.17	0.076
Ag/AgCl	2.365	7.389	0.543	27.05	0.085

4. Discussion

This study has shown that an Ag/AgCl RE can be electroplated on to an Al bond-pad of a TSMC 0.18 μm CMOS microchip and it can provide a stable potential. The observed drift rate of 0.3 mV/h is comparable to other thin-film Ag/AgCl QREs without dissolution-limiting coatings in the literature, which are collated in Table 3. Of particular note is the lower drift rate of the electroplated QRE compared to that in Kumashi et al., which used sputtering to produce an Ag/AgCl QRE on a CMOS bond-pad. This demonstrates that the electroplated QRE not only produces benefits in terms of manufacturing, but can also perform better than sputtered counterparts. The electroplated QRE in this study also performs similarly to or better than other QREs whose fabrication process includes electroplating. The lifetime of the plated QRE, which extends over 18 h, is sufficiently long for the many electrochemical sensing applications.

The CV analysis of the final Ag/AgCl electrode could point towards slow electron transfer properties. This is not ideal, but acceptable for a proof-of-concept, with further optimisation of the electrode required moving forwards. The problem likely stems from the Ag/AgCl layer, as the underlying ENIG layer demonstrated relatively quick electron transfer. It is possible that a highly porous Ag surface may be beneficial to QRE performance [32]. By having a larger surface area in contact with the electrolyte, the exchange of Cl ions can occur at a greater rate, allowing the QRE to react more quickly to changes in local Cl ion concentration and thus keep a more stable potential. It is worth investigating whether a constantly applied electroplating current would create a more porous Ag/AgCl layer and improve electrode performance.

The ENIG plating progressed well, as evidenced by the 'bump' profile obtained and the CV analysis. However, a number of ENIG-plated pads failed adhesion tests, with the ENIG layer or the underlying Al pad delaminating. It was noted that adhesion test performance was worse for pads with a bump-profile or where thermal regulation of plating baths was sub-optimal. Thermal regulation of the plating baths would be more straightforward with specialised tanks and immersion heaters, which is an advantage of scaling up the process. The bump-profile is also unnecessary for QRE functionality and thus shorter Ni plating times should be used. Shorter etching times of the Al pad and zincated layers or more diluted etchants should be used to avoid Al delamination.

Whilst the fabrication process presented in this work contained a step requiring an electrical connection to the chip, the vision is to have a fully electroless process. With this approach, creation of QREs on CMOS chips would simply require immersion of a wafer into a sequence of different chemicals. Such a process could be significantly scaled up to a multi-wafer level process; As many wafers as can fit in the chemical tank can be plated at once, far outstripping the production capability of other thin-film Ag/AgCl REs. To realise this vision, an autocatalytic electroless Ag plating solution must become commercially available.

An electroless process would lack specificity in the bond-pads that are plated. As such, it is wireless chips, which do not require wire-bonded connections, containing sensors such as FETs and ISFETs, where only the RE is exposed to the electrolyte, that stand to benefit most from an electroless RE fabrication process.

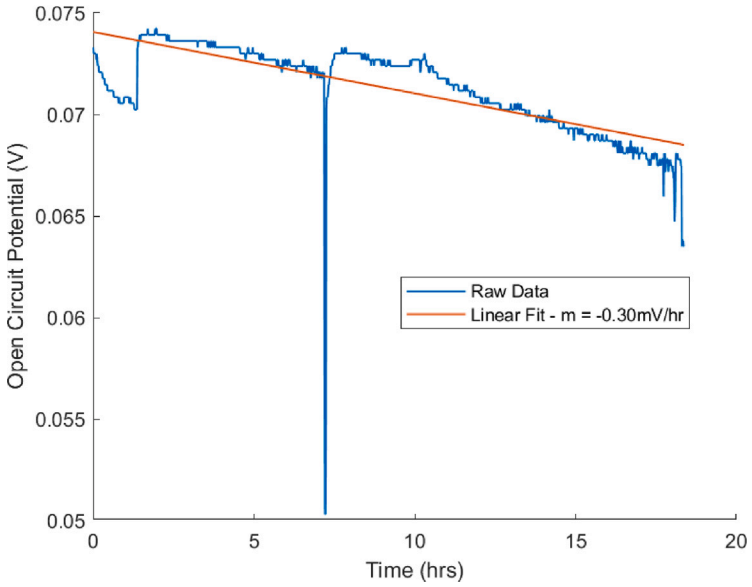

Fig. 6. A graph of OCP versus time for the plated Ag/AgCl electrode measured against a commercial Ag/AgCl glass electrode in 100 mM KCl solution over an 18-hour period. A linear fit is provided, along with the drift rate of OCP that it represents. The large discontinuity at around 7 h is assumed to be cause by bubble formation and the point is omitted from the linear fit.

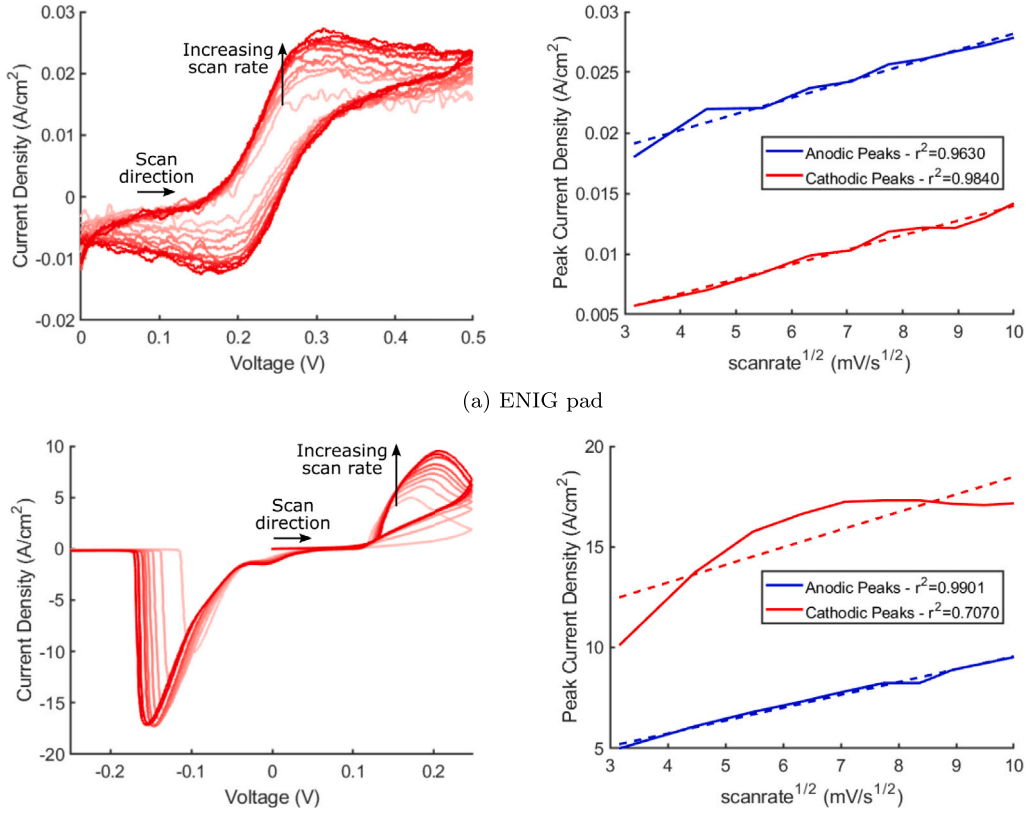

(a) ENIG pad

(b) *AgCl* pad

Fig. 7. CV analysis for the (**a**) ENIG-plated pad and (**b**) AgCl-plated pad. (**left**) Graphs of five-point moving means of CV curves using a commercial Ag/AgCl RE and Pt mesh CE in 0.1 M KCl, 0.1 mM K_3FeCN_6, and 1 mM K_4FeCN_6. 10 scan rates from 10–100 mV/s were run. Increasing scan rate direction is shown by increasing opacity of the line and is annotated on the graphs, along with the direction of the scans. (**right**) Graphs of absolute peak cathodic (**red**) and anodic (**blue**) current against the square-root of scan rate. Linear fits are provided, along with their r^2 values.

5. Conclusion

In this study, the metal bond-pads of a commercial CMOS process were used as a base to create an electroplated Ag/AgCl QRE for the first time. Industry-standard zincate and ENIG electroless surface processing was conducted on the Al pads to provide a Au surface on to which Ag was electroplated and then chlorinated. The final Ag/AgCl electrode was able to sustain an OCP on the order of 10 mV for up to 18 h with

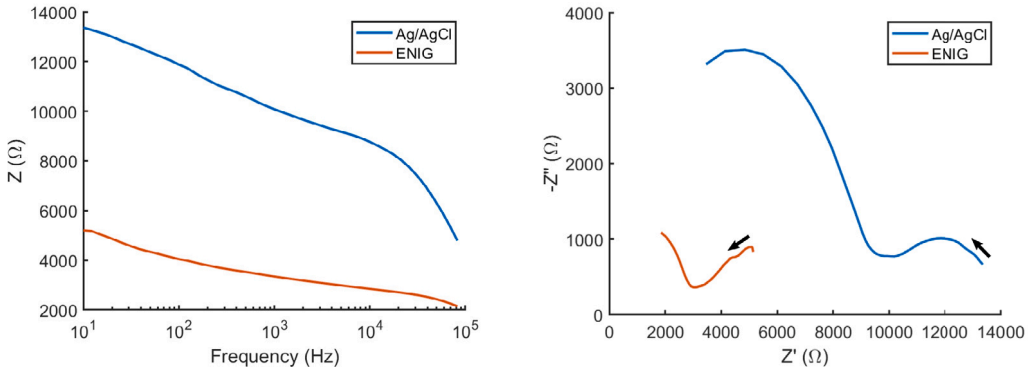

(a) Bode (b) Nyquist

Fig. 8. (**a**) Bode and (**b**) Nyquist plots of the impedance spectra of the (**red**) ENIG and (**blue**) Ag/AgCl-plated pads, measured in 100 mM KCl with a Pt mesh CE and commercial Ag/AgCl RE with a 5 mV excitation signal ranging from 10 Hz - 100 kHz. The black arrows in (**b**) represent the direction from low to high frequency.

Table 3
A table comparing the performance of thin-film Ag/AgCl QREs in the literature that do not use a dissolution-limiting coating and that have been electrochemically characterised with the QRE fabricated as part of this study. S = Sputtering, Ev = Evaporation, El = Electroplating.

Year	Paper	Fabrication	Potential (mV)	Drift (mV/h)	Measurement Time (h)	On-CMOS
2006	Polk et al. [25]	S, El	32–42	0.12	16.7 (Up to 96)	✗
2010	Zhou et al. [33]	S, El	230	0.625	8	✗
2013	Schnitker et al. [34]	Ev, El	−83–85	1.48	6	✗
	Baraket et al. [35]	S, El	−105–110	0.2	13	✗
2017	Rahman et al. [36]	S	−1–3	0.2	48	✗
2018	Hoa et al. [37]	Ev, El	-	0.1	24	✗
2019	Wang et al. [38]	S, Ev	-	0.457	10	✗
2021	Dai et al. [8]	S, El	338.2 - 336.7	0.6	10	✗
	Kumashi et al. [7]	S	230 - 190	1.4	48	✓
2023	**This work**	**El**	**75 - 65**	**0.3**	**18**	✓

a drift rate of 0.3 mV/h, which is comparable to thin-film REs in the literature. This provides the basis for a fully electroless process that will be able to create on-chip Ag/AgCl electrodes on a multi-wafer scale.

Declaration of competing interest

The authors declare the following financial interests/personal relationships which may be considered as potential competing interests: Lewis Keeble reports financial support was provided by EPSRC Centre for Doctoral Training in High Performance Embedded and Distributed Systems. Arthur Jaccottet reports financial support was provided by Swiss-European Mobility Programme - Student Mobility for Studies. Prof. Pantelis Georgiou and Dr. Jesus Rodriguez Manzano are founders of Proton Dx, currently acting as CEO and CSO respectively. If there are other authors, they declare that they have no known competing financial interests or personal relationships that could have appeared to influence the work reported in this paper.

Data availability

Data will be made available on request.

Acknowledgements

The authors would like to thank the High Performance Embedded and Distributed Systems (HiPEDS) EPSRC Centre for Doctoral Training (EP/L016796/1) at Imperial College London for supporting this work. Electroless plating was conducted at the Bionanofabrication Cleanroom, Bioengineering Department, Imperial College London. Electroplating and electrochemical characterisation was conducted at the Centre for Bio-inspired Technology Cleanroom, Electrical and Electronic Engineering Department, Imperial College London. SEM characterisation was performed at the Hamlyn Centre, Department of Electrical and Electronic Engineering, Imperial College London.

Appendix A. Supplementary data

Supplementary material related to this article can be found online at https://doi.org/10.1016/j.electacta.2024.143780.

References

[1] J. Baranwal, B. Barse, G. Gatto, G. Broncova, A. Kumar, Electrochemical sensors and their applications: A review, Chemosensors 10 (9) (2022) 363, http://dx.doi.org/10.3390/CHEMOSENSORS10090363.

[2] P.S. Singh, From sensors to systems: CMOS-integrated electrochemical biosensors, IEEE Access 3 (2015) 249–259, http://dx.doi.org/10.1109/ACCESS.2015.2410256.

[3] H. Li, X. Liu, L. Li, X. Mu, R. Genov, A.J. Mason, CMOS electrochemical instrumentation for biosensor microsystems: A review, Sensors 17 (1) (2017) http://dx.doi.org/10.3390/S17010074.

[4] M.W. Shinwari, D. Zhitomirsky, I.A. Deen, P.R. Selvaganapathy, M.J. Deen, D. Landheer, Microfabricated reference electrodes and their biosensing applications, Sensors 10 (3) (2010) 1679–1715, http://dx.doi.org/10.3390/s100301679.

[5] K.S. Yun, J. Gil, J. Kim, H.J. Kim, K. Kim, D. Park, M.S. Kim, H. Shin, K. Lee, J. Kwak, E. Yoon, A miniaturized low-power wireless remote environmental monitoring system based on electrochemical analysis, Sensors Actuators, B: Chem. 102 (1) (2004) 27–34, http://dx.doi.org/10.1016/J.SNB.2003.11.008.

[6] J. Zhang, Y. Huang, N. Trombly, C. Yang, A. Mason, Electrochemical array microsystem with integrated potentiostat, IEEE Sensors (2005) 385–388., http://dx.doi.org/10.1109/ICSENS.2005.1597716.

[7] S. Kumashi, D. Jung, J. Park, S. Tejedor-Sanz, S. Grijalva, A. Wang, S. Li, H.C. Cho, C. Ajo-Franklin, H. Wang, A CMOS multi-modal electrochemical and impedance cellular sensing array for massively paralleled exoelectrogen screening, IEEE Trans. Biomed. Circuits Syst. 15 (2) (2021) 221–234, http://dx.doi.org/10.1109/TBCAS.2021.3068710.

[8] J. Dai, W. Gao, J. Yin, L. Liang, J. Zou, Q. Jin, Microfluidic sensor integrated with nanochannel liquid conjunct Ag/AgCl reference electrode for trace Pb(II) measurement, Anal. Chim. Acta 1164 (2021) http://dx.doi.org/10.1016/J.ACA.2021.338511.

[9] V. Torres-González, J.A. Ávila-Niño, E. Araujo, Facile fabrication of tailorable Ag/AgCl reference electrodes for planar devices, Thin Solid Films 757 (2022) http://dx.doi.org/10.1016/J.TSF.2022.139413.

[10] P. Tirado, I.R. Chavez-Urbiola, J.J. Alcantar-Peña, Ionic gel effect on a reference electrode in a flexible solid-state pH sensor, MRS Commun. 13 (1) (2022) 41–46, http://dx.doi.org/10.1557/S43579-022-00309-Y/TABLES/1.

[11] E.T.S.G.D. Silva, S. Miserere, L.T. Kubota, A. Merkoçi, Simple on-plastic/paper inkjet-printed solid-state Ag/AgCl pseudoreference electrode, Anal. Chem. 86 (21) (2014) 10531–10534, http://dx.doi.org/10.1021/AC503029Q/SUPPL_FILE/AC503029Q_SI_001.PDF.

[12] S. Papamatthaiou, U. Zupancic, C. Kalha, A. Regoutz, P. Estrela, D. Moschou, Ultra stable, inkjet-printed pseudo reference electrodes for lab-on-chip integrated electrochemical biosensors, Sci. Rep. 10 (1) (2020) 1–10, http://dx.doi.org/10.1038/s41598-020-74340-1.

[13] A. Moya, R. Pol, A. Martínez-Cuadrado, R. Villa, G. Gabriel, M. Baeza, Stable full-inkjet-printed solid-state Ag/AgCl reference electrode, Anal. Chem. 91 (24) (2019) 15539–15546, http://dx.doi.org/10.1021/ACS.ANALCHEM.9B03441.

[14] W.-Y. Liao, T.-C. Chou, Fabrication of a planar-form screen-printed solid electrolyte modified Ag/AgCl reference electrode for application in a potentiometric biosensor, Anal. Chem. 78 (12) (2006) 4219–4223, http://dx.doi.org/10.1021/ac051562.

[15] D. Moschou, T. Trantidou, A. Regoutz, D. Carta, H. Morgan, T. Prodromakis, Surface and electrical characterization of Ag/AgCl pseudo-reference electrodes manufactured with commercially available PCB technologies, Sensors 15 (8) (2015) 18102–18113, http://dx.doi.org/10.3390/s150818102.

[16] T. Luo, H. Wang, H. Song, J.B. Christen, CMOS-based on-chip electrochemical sensor, in: 2014 IEEE Biomedical Circuits and Systems Conference (BioCAS) Proceedings, 2014, pp. 336–339, http://dx.doi.org/10.1109/BioCAS.2014.6981731.

[17] H. Yin, X. Mu, H. Li, X. Liu, A.J. Mason, CMOS monolithic electrochemical gas sensor microsystem using room temperature ionic liquid, IEEE Sensors 18 (19) (2018) 7899–7906, http://dx.doi.org/10.1109/JSEN.2018.2863644.

[18] U. Frey, J. Sedivy, F. Heer, R. Pedron, M. Ballini, J. Mueller, D. Bakkum, S. Hafizovic, F.D. Faraci, F. Greve, K.-U. Kirstein, A. Hierlemann, Switch-matrix-based high-density microelectrode array in CMOS technology, IEEE J. Solid-State Circuits 45 (2) (2010) 467–482, http://dx.doi.org/10.1109/JSSC.2009.2035196.

[19] H.R. Lim, N. Hillman, Y.T. Kwon, Y.S. Kim, Y.H. Choa, W.H. Yeo, Ultrathin, long-term stable, solid-state reference electrode enabled by enhanced interfacial adhesion and conformal coating of AgCl, Sensors Actuators, B: Chem. 309 (2020) 127761, http://dx.doi.org/10.1016/j.snb.2020.127761.

[20] Q. Li, W. Tang, Y. Su, Y. Huang, S. Peng, B. Zhuo, S. Qiu, L. Ding, Y. Li, X. Guo, Stable thin-film reference electrode on plastic substrate for all-solid-state ion-sensitive field-effect transistor sensing system, IEEE Electron Device Lett. 38 (10) (2017) 1469–1472, http://dx.doi.org/10.1109/LED.2017.2732352.

[21] R. Mamińska, A. Dybko, W. Wróblewski, All-solid-state miniaturised planar reference electrodes based on ionic liquids, Sensors Actuators, B: Chem. 115 (1) (2006) 552–557, http://dx.doi.org/10.1016/j.snb.2005.10.018.

[22] D. Ma, S.S. Ghoreishizadeh, P. Georgiou, DAPPER: A low power, dual amperometric and potentiometric single-channel front end, in: 2020 IEEE International Symposium on Circuits and Systems, ISCAS, 2020, pp. 1–5, http://dx.doi.org/10.1109/ISCAS45731.2020.9181213.

[23] J. Burgess, Electroplating onto aluminium and its alloys, Trans. IMF 97 (6) (2019) 285–288, http://dx.doi.org/10.1080/00202967.2019.1675280.

[24] D.A. Hutt, C. Liu, P.P. Conway, D.C. Whalley, S.H. Mannan, Electroless nickel bumping of aluminum bondpads - Part I: Surface pretreatment and activation, IEEE Trans. Compon. Packag. Technol. 25 (1) (2002) 87–97, http://dx.doi.org/10.1109/6144.991180.

[25] B.J. Polk, A. Stelzenmuller, G. Mijares, W. MacCrehan, M. Gaitan, Ag/AgCl microelectrodes with improved stability for microfluidics, Sensors Actuators, B: Chem. 114 (1) (2006) 239–247, http://dx.doi.org/10.1016/j.snb.2005.03.121.

[26] C.L. Hsu, A. Sun, Y. Zhao, E. Aronoff-Spencer, D.A. Hall, A 16×20 electrochemical CMOS biosensor array with in-pixel averaging using polar modulation, in: 2018 IEEE Custom Integrated Circuits Conference, Institute of Electrical and Electronics Engineers Inc., 2018, pp. 1–4, http://dx.doi.org/10.1109/CICC.2018.8357044.

[27] J.S. Park, S.I. Grijalva, D. Jung, S. Li, G.V. Junek, T. Chi, H.C. Cho, H. Wang, Intracellular cardiomyocytes potential recording by planar electrode array and fibroblasts co-culturing on multi-modal CMOS chip, Biosens. Bioelectron. 144 (2019) 111626, http://dx.doi.org/10.1016/J.BIOS.2019.111626.

[28] B.J. Polk, M. Bernard, J.J. Kasianowicz, M. Misakian, M. Gaitan, Microelectroplating silver on sharp edges toward the fabrication of solid-state nanopores, J. Electrochem. Soc. 151 (9) (2004) 559, http://dx.doi.org/10.1149/1.1773732.

[29] N.N. Elgrishi, K.J. Rountree, B.D. Mccarthy, E.S. Rountree, T.T. Eisenhart, J.L. Dempsey, A practical beginner's guide to cyclic voltammetry, 2017, http://dx.doi.org/10.1021/acs.jchemed.7b00361.

[30] R.S. Nicholson, Semiempirical procedure for measuring with stationary electrode polarography rates of chemical reactions involving the product of electron transfer, Anal. Chem. 38 (10) (1966) 1406, http://dx.doi.org/10.1021/AC60242A030/ASSET/AC60242A030.FP.PNG_V03.

[31] K.C.E. Tjon, J. Yuan, Impedance characterization of silver/silver chloride microelectrodes for bio-sensing applications, Electrochim. Acta 320 (2019) http://dx.doi.org/10.1016/J.ELECTACTA.2019.134638.

[32] B. Rostami, S.I. Mirzaei, A. Zamani, A. Simchi, M. Fardmanesh, Development of an enhanced porosity AgAgCl reference electrode with improved stability, Eng. Res. Express 1 (1) (2019) 015039, http://dx.doi.org/10.1088/2631-8695/ab4544.

[33] J. Zhou, K. Ren, Y. Zheng, J. Su, Y. Zhao, D. Ryan, H. Wu, Fabrication of a microfluidic Ag/Agcl reference electrode and its application for portable and disposable electrochemical microchips, ELECTROPHORESIS 31 (18) (2010) 3083–3089, http://dx.doi.org/10.1002/elps.201000113.

[34] J. Schnitker, D. Afanasenkau, B. Wolfrum, A. Offenhäusser, Planar reference electrodes on multielectrode arrays for electrochemical measurements of ionic currents, Physica Status Solidi (a) 210 (5) (2013) 892–897, http://dx.doi.org/10.1002/pssa.201200850.

[35] A. Baraket, M. Lee, N. Zine, M. Sigaud, N. Yaakoubi, M.G. Trivella, M. Zabala, J. Bausells, N. Jaffrezic-Renault, A. Errachid, Diazonium modified gold microelectrodes onto polyimide substrates for impedimetric cytokine detection with an integrated Ag/AgCl reference electrode, Sensors Actuators, B: Chem. 189 (2013) 165–172, http://dx.doi.org/10.1016/j.snb.2013.02.088.

[36] T. Rahman, T. Ichiki, Fabrication and characterization of a stabilized thin film Ag/AgCl reference electrode modified with self-assembled monolayer of alkane thiol chains for rapid biosensing applications, Sensors 17 (2017) 2326, http://dx.doi.org/10.3390/s17102326, URL http://www.mdpi.com/1424-8220/17/10/2326.

[37] L.N.Q. Hoa, H.-R. Chen, T.T.-C. Tseng, An arrayed micro-glutamate sensor probe integrated with on-probe Ag/AgCl reference and counter electrodes, Electroanalysis 30 (3) (2018) 561–570, http://dx.doi.org/10.1002/elan.201700762.

[38] N. Wang, E. Kanhere, K. Tao, L. Hu, J. Wu, J. Miao, M.S. Triantafyllou, Investigation of a thin-film quasi-reference electrode fabricated by combined sputtering-evaporation approach, Electroanalysis 31 (3) (2018) 560–566, http://dx.doi.org/10.1002/elan.201800532.